THEORETICAL AND APPLIED MECHANICS
Volume 48 (2021) Issue 2, 143–157 DOI: https://doi.org/10.2298/TAM211011008S

TOWARDS VIABLE FLOW SIMULATIONS OF SMALL-SCALE ROTORS AND BLADE SEGMENTS

Jelena Svorcan, Aleksandar Kovačević, Dragoljub Tanović, and Mohammad Sakib Hasan

Abstract. The paper focuses on the possibilities of adequately simulating complex flow fields that appear around small-scale propellers of multicopter aircraft. Such unmanned air vehicles (UAVs) are steadily gaining popularity for their diverse applications (surveillance, communication, deliveries, etc.) and the need for a viable (i.e. usable, satisfactory, practical) computational tool is also surging. From an engineering standpoint, it is important to obtain sufficiently accurate predictions of flow field variables in a reasonable amount of time so that the design process can be fast and efficient, in particular the subsequent structural and flight mechanics analyses. That is why more or less standard fluid flow models, e.g. Reynolds-averaged Navier–Stokes (RANS) equations solved by the finite volume method (FVM), are constantly being employed and validated. On the other hand, special attention must be given to various flow peculiarities occurring around the blade segments shaped like airfoils since these flows are characterized by small chords (length-scales), low speeds and, therefore, low Reynolds numbers (Re) and pronounced viscous effects. The investigated low-Re flows include both transitional and turbulent zones, laminar separation bubbles (LSBs), flow separation, as well as rotating wakes, which require somewhat specific approaches to flow modeling (advanced turbulence models, fine spatial and temporal scales, etc). Here, the conducted computations (around stationary blade segments as well as rotating rotors), closed by different turbulence models, are presented and explained. Various qualitative and quantitative results are provided, compared and discussed. The main possibilities and obstacles of each computational approach are mentioned. Where possible, numerical results are validated against experimental data. The correspondence between the two sets of results can be considered satisfactory (relative differences for the thrust coefficient amount to 15%, while they are even lower for the torque coefficient). It can be concluded that the choice of turbulence modeling (and/or resolving) greatly affects the final output, even in design operating conditions (at medium angles-of-attack where laminar, attached flow dominates). Distinctive flow phenomena still exist, and in order to be adequately simulated, a comprehensive modeling approach should be adopted.

2020 *Mathematics Subject Classification:* 76D05; 76F06; 76M12.
Key words and phrases: CFD, turbulence, propeller, airfoil.

1. Introduction

The paper investigates fluid flows around propellers of small-scale multicopter UAVs in both design and off-design operating conditions. UAVs are so popular today for their ability to hover as well as perform progressive flight and accomplish various useful assignments (monitoring, observation, reporting, delivering, cleaning, enabling communication, etc.) that require significant flying maneuverability. These aircraft are usually equipped with fixed-geometry propellers that are controlled solely by changing their angular velocities. In order to provide fast responses to the desired flying commands, their rotors must be able to produce satisfactory levels of thrust and torque in all operating conditions, both nominal (e.g. at 70%) and off-design (at low angular velocities). In other words, the fluid flow around the propeller rotors (including blade segments) should be known or estimated sufficiently accurately, which particularly applies to hover, the basic axisymmetric flying condition.

This study focuses on a propeller blade intended for a quadcopter with the 10-15 kg useful payload that was specially designed for the following working regime – angular velocity $\Omega = 3289$ rpm corresponding to the 70% engine (electric motor) throttle. The blade shape (airfoil contour) was obtained through an optimization study [**1**] that required a simple and fast estimation of propeller thrust and torque at a nominal Reynolds number of 300,000 (while off-design conditions correspond to the range 60,000-200,000 of Re). Although various numerical models, differing in complexity and the amount of physical details they take into account, exist and are regularly employed [**2**–**5**], a combined blade element momentum theory (BEMT), which uses simplified 2D aerodynamic characteristics, is still the most suitable for preliminary analysis and a large number of repeated computations [**2**–**4**], while the computational fluid dynamics (CFD) approach is used in subsequent design phases for a more detailed inspection of flow field variables. CFD analyses should be able to incorporate viscous effects to the highest degree and therefore provide the most accurate output data.

However, low-Re flows around propeller blades, even at medium angles-of-attack (α, AoAs), are intriguing and complicated for simulation since numerous flow peculiarities appear, e.g. initially laminar flow transits to turbulent through laminar separation bubbles (LSBs) which can even be accompanied by massive flow separation. These mechanisms still remain unresolved and different numerical approaches have to be tried and their applicability estimated [**6**–**11**].

In continuation, some comments on usually employed approaches to turbulence modeling are provided. To be as comprehensive and useful as possible, the core of this investigation comprises two parts:

- numerical simulation of the flow around a stationary blade segment,

and

- numerical simulation of the flow around the whole rotor,

which are described in more detail in the following sections. In the end, a brief summary, some conclusions and few recommendations are given.

2. A few comments on turbulence modeling

While (Unsteady) Reynolds-averaged Navier–Stokes or (U)RANS equations describing the fluid flow are still dominantly used in industrial applications [**9**–**11**], certain models that resolve at least a portion of the turbulence spectrum (i.e. scale-resolving or SR) are becoming more and more employed, even though they are extremely computationally expensive [**6**,**8**,**9**]. The main reason for their increased use is their ability to better describe real physical processes (in particular energy dissipation) since they take into account more fluid flow information (that we otherwise consider as noise). However, the appropriateness and accuracy of numerical results obtained by more advanced turbulence models is still questionable, and should be investigated in detail. It is therefore best to begin with relatively familiar examples such as external flows around airfoils (i.e. wing or blade segments in 3D) and perform a comparative study of the obtained results.

Additional complication in wall bounded flows is that they incorporate extremely small turbulence length scales (particularly in the wall vicinity) that also decrease at higher Re [**9**]. Generally, linear dependence of the turbulent length scale L on the wall distance y can be assumed, except in the viscous sublayer where turbulence is damped by the dominant effects of molecular viscosity μ. Given that the thickness of the viscous sublayer is greater at low-Re, it is generally easier to numerically simulate (and partially resolve) such flows. On the other hand, laminar-turbulent transition highly complicates everything and makes simulating the low-Re cases almost equally unfavorable as high-Re.

Here, together with transition SST (or $\gamma - \mathrm{Re}_\theta$) [**7**], a hybrid Scale-Adaptive Simulation (SAS) model [**8**, **9**], which resolves large eddies far away from the walls while the flow in the wall vicinity (boundary layer) is modeled by the RANS approach, was employed for the case of a single blade segment. In order to obtain results of the highest possible accuracy and gain insight into the modeling capabilities of flows around airfoils at low-Re, the authors tried and compared several computational approaches differing in complexity. They started with XFoil [**12**], a panel method enhanced by various corrections that incorporate viscous effects, performed both 2D and 3D flow simulations by transition SST turbulence model [**7**], and ultimately employed one of the more advanced turbulence models available in ANSYS Fluent – transitional SST-SAS [**8**, **9**]. SAS implies the safest (most conservative) approach since it should revert back to (U)RANS if the mesh (i.e. length) or temporal resolution is insufficient. Here, at lower AoAs, the flow is mostly locally unstable as turbulence in the boundary layer primarily dictates the flow around the airfoil (i.e. the streamlined body). At higher AoAs, the turbulent mixing of boundary layers coming from the lower and upper airfoil sides also becomes significant. As stated in [**9**], SAS may not be the most adequate choice in such flow cases, and other scale resolving models should be used instead.

One possibility that still requires enormous computing power but should be tried in future studies (when more computational resources are at disposal) is certainly Large Eddy Simulation (LES). It is one of the most promising and employed SR models that resolves larger scales of turbulence while filtering/removing the

smallest scale information. At length-scales that correspond to the grid size, turbulence can be considered isotropic and homogeneous and a flow must be modeled [**9**]. In this case, it means that the numerical grid near the walls should be very fine to resolve the smallest scales of turbulence in the boundary layer, which is computationally very expensive. Furthermore, LES has not yet reached a level of maturity that enables the users without significant experience and knowledge of flow physics to obtain sufficiently accurate and reliable results [**13**].

On the other hand, in the second case where the whole rotor is investigated, a standard, quasi-steady approach that combines RANS equations closed by the $k-\omega$ SST turbulence model with the multiple reference frames (MRF) is adopted [**6**] to account for both turbulence and rotating effects. This was primarily done because of relatively limited computational resources that had to be employed when solving such complex flows.

3. Flow around a blade segment

We start the propeller analysis with the inspection of its single section to better understand the complex flow physics and precisely determine how well it can be simulated. As previously mentioned, the contour of the investigated airfoil, illustrated in Fig. 1, was defined after a multi-objective optimization study that was performed in order to obtain the best aerodynamic performances of the propeller [**1**]. Since this was part of the conceptual design, the airfoil itself was not experimentally investigated, but only numerically, at the assumed Reynolds number of 300,000. Since no universal turbulence model can be applied to all industrial flows, different models were tried in order to obtain the most usable results.

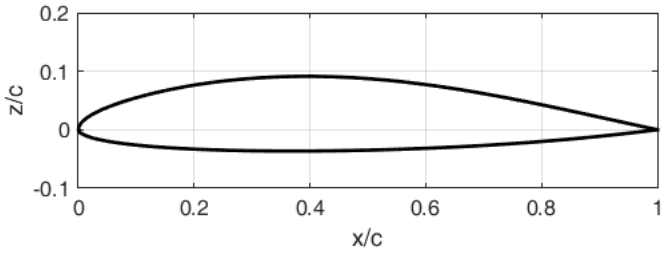

FIGURE 1. Airfoil contour

An interesting flow phenomenon should be introduced here. Laminar separation bubbles (LSBs), i.e. small zones of recirculating flow adjacent to wall surfaces appearing at low Reynolds numbers, lead to laminar-to-turbulent transition, instigate increased noise and vibrations and may lead to decreased aerodynamic performances. Thus, they have been much investigated in the past decades, both experimentally and numerically [**14**–**16**]. However, vortex formation and breakdown processes typical of LSB development still remain insufficiently resolved. This is probably due to their sensitivity to the disturbance environment, as well as numerous difficulties in performing experimental measurements that do not change

the nature of the flow [**14**]. On the other hand, accurate estimation of laminar-to-turbulent transition greatly facilitates accurate prediction of the skin-friction coefficient (and vice versa). Both of the mentioned characteristics directly affect the drag coefficient and overall aerodynamic efficiency. For these reasons, further research into LSBs is necessary, and a small portion of it is included in this study.

3.1. Geometry of the computational domain. Computational domain is formed from a half-circle (extending $12.5c$ around the airfoil) and an aft rectangle (spanning $20c$ behind the airfoil) as presented in Fig. 2. In the span-wise direction, the domain extent is one chord-length c, which is sufficient for allowing turbulent structures to develop (without the effects of side boundaries).

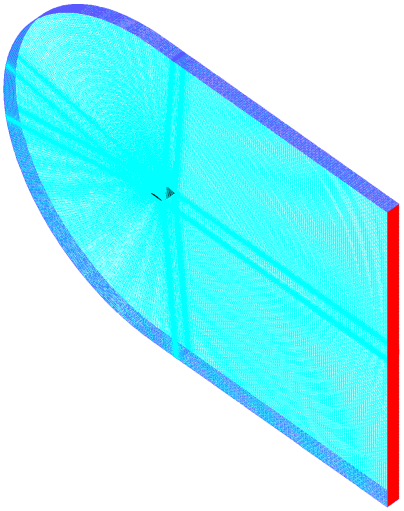

FIGURE 2. Extents of the computational domain with outer boundaries

The inlet boundaries are colored dark blue, the outlet boundary red, while the pair of periodic, side surfaces is colored light blue. A small blade segment is barely visible in the center of the computational domain.

3.2. Computational grid. Generation of high-quality mesh is quite an important, but also a challenging task. When possible, a traditional approach should be adopted, similar to [**17**, **18**]. Initial fine, planar mesh was C-type structured, while its 3D counterpart is obtained by extruding 40 cells in a span-wise direction. The dimensionless wall distance y^+ is lower than 0.5 along the whole airfoil, while the cell growth ratio never exceeds 1.2. Unfortunately, main limitations to further mesh refinement are the available computational resources. The overall number of cells is approximately 4 million. Illustrations of the generated and used computational grid around the airfoil together with its details near the airfoil leading and trailing edges are provided in Fig. 3.

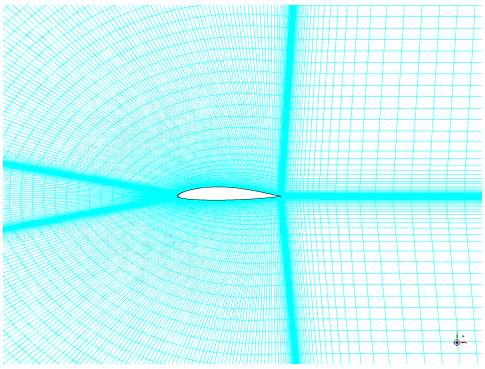

FIGURE 3. Detail of the generated mesh around the airfoil

3.3. Numerical set-up. All flow simulations were performed in ANSYS Fluent [**6**], where the governing equations for spatial, incompressible, viscous, both steady and transient (where necessary, at certain AoAs) flow are solved by the finite volume method (FVM).

As previously stated, a Reynolds number of Re = 300,000 determined the flow conditions. For the airfoil chord length $c = 1$ m and standard air conditions (i.e. values of density ρ and viscosity μ in accordance with the standard atmosphere model), the free-stream velocity magnitude defined along the inlet boundary was $V_o = 4.3822$ m/s, while its direction is determined by AoA. Zero gauge pressure is assumed along the outlet. Periodic boundary conditions are applied on the side surfaces (since symmetry may appear nonphysical in the case of turbulent flows). Flow equations are closed by one of the previously mentioned turbulence models.

A pressure-based solver with SIMPLEC pressure-velocity coupling scheme is used. All spatial and temporal (where applicable) discretizations are at least 2nd order. In the unsteady simulations, the assumed time-step is 1 ms, producing a Courant number CFL ≈ 1. Computations were performed until the convergence of aerodynamic coefficients was achieved.

3.4. Results and discussion. Computed velocity contours around the airfoil at two different AoAs, namely $\alpha = 0°$ and $\alpha = 8°$, are provided in Fig. 4. Large-scale flow features such as the fore stagnation point, flow acceleration along the upper boundary (and deceleration along the lower side), relatively narrow wake detaching from the trailing edge (that expands at higher AoAs), etc. are clearly visible. Given that the flow remains smooth and attached over a wide range of AoA, it may be concluded that the airfoil is suitable for the designed operating conditions.

However, in order to inspect in more detail small-scale flow features, such as LSBs and other boundary layer occurrences, it is necessary to come very close to the airfoil walls. The topology of computed LSBs, i.e. their size and location at various AoAs, can be deduced from the functions of two standard dimensionless variables – pressure C_p and skin-friction C_f coefficient distributions along the upper

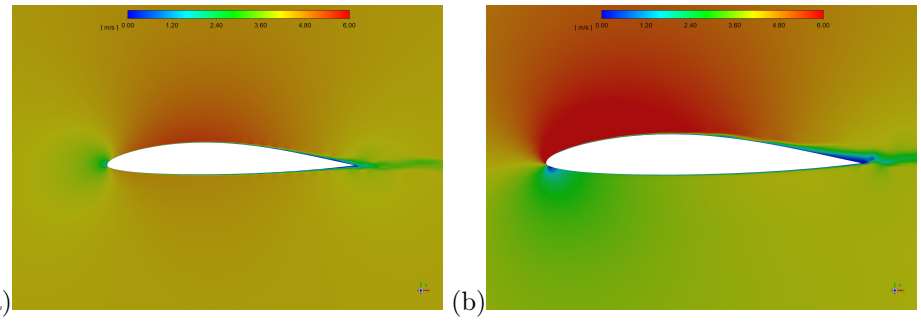

(a) (b)

FIGURE 4. Velocity contours at: (a) $\alpha = 0°$, (b) $\alpha = 8°$

surface that are illustrated in Fig. 5. Generally, LSBs are denoted by even pressure (zone of reversed flow) followed by the sudden pressure jump which is induced by the flow reattachment. Here, however, due to the dynamic behavior of the LSB, which actually comprises numerous smaller bubbles that interact, a zone of varying pressure coefficient is easily recognized. The same range of the relative longitudinal coordinate x/c corresponds to the alternating negative and positive values of the skin-friction coefficient that imply to the small zones of reversed flow at all AoAs. However, it should be mentioned that LSBs are inherent characteristics of the employed transition SST turbulence model and that their computation is highly governed by it. At $\alpha = 0°$ LSBs begin to appear in the second half, i.e. at $x/c > 0.5$. With the increase in AoA, their occurrences slowly move forward, towards the airfoil nose. Ultimately, at $\alpha = 8°$, a small LSB even appears in the region $0.03 < x/c < 0.07$. However, it quickly dies out, the flow remains laminar (induced by observing intermittency distribution not represented here) and the next flow reversal happens at $x/c > 0.4$.

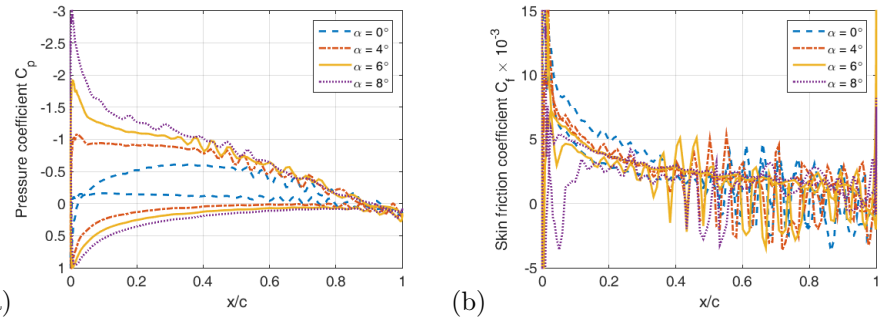

(a) (b)

FIGURE 5. (a) Pressure coefficient, and (b) skin friction coefficient distributions

Inside the LSB, the values of turbulence kinetic energy (TKE) k and turbulent dissipation rate ϵ are smaller than the adjacent up- and downstream, while the

contrary can be said for the values of specific dissipation rate ω. The obtained values of intermittency γ indicate a purely laminar flow inside the LSB.

Laminar-turbulent transition (triggered by the laminar separation bubble) can clearly be seen by turbulence structures illustrated in Fig. 6. Their dimension increases in the flow direction, particularly after the trailing edge. As AoA increases, vivid and picturesque turbulence structures move forward and become more scattered (dissipated).

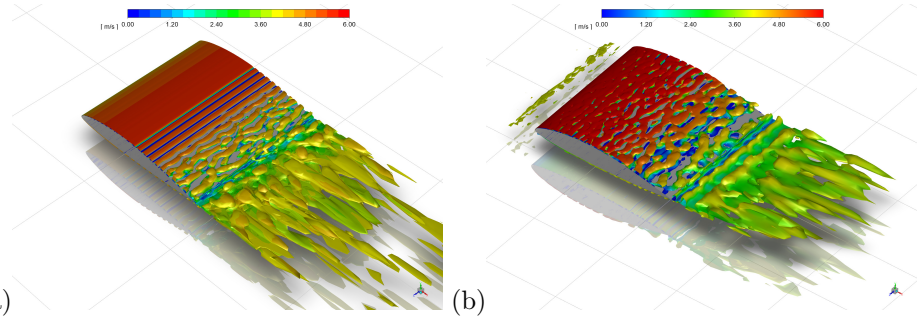

FIGURE 6. Turbulence iso-structures around the blade segment at: (a) $\alpha = 0°$, (b) $\alpha = 8°$

3.5. Validation of the computational models. Unfortunately, since no experimental data is available, critical estimate of the computational models is performed thorough their mutual comparison as well as correlation to the numerical results obtained by a simpler aerodynamic model (potential flow enhanced by semi-empirical corrections solved by a panel method) in the freely available tool XFoil [**12**]. The results of both 3D analyses mostly lie somewhere between the curves obtained by a panel method and 2D CFD simulations, see Fig. 7. Linearity of the lift curve obtained by transition SST-SAS seems to be preserved, while all other models seem to enter the non-linear range at $\alpha > 6°$. Drag is by far the highest in the 2D CFD simulations, while the transition SST-SAS model provides lower values than the 3D transition SST, which ultimately results in an improved lift-to-drag ratio, particularly at $\alpha = 8°$.

What happens at higher AoAs should be investigated in a future study (where experimental validation would be the best). Also, aerodynamic coefficient amplitudes seem to reduce at higher AoA for the transition SST-SAS turbulence model, indicating (and confirming) that this model is more suitable for globally unstable flows (than for small local instabilities where DES should better be employed).

4. Flow around a small-scale propeller

The geometry of the investigated small-scale propeller is relatively simple. A constant airfoil together with linear pitch and cubic chord distributions is applied along the streamlined portion of the blade. The rotor diameter is $D = 0.76$ m. This

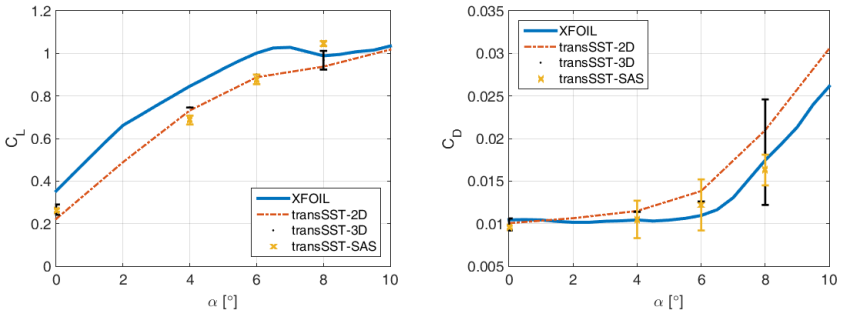

FIGURE 7. Computed aerodynamic coefficients

light-weight blade, of composite sandwich structure, was manufactured by one of the authors.

4.1. Geometry of the computational domain. As illustrated in Fig. 8, the complete geometry was modeled (and not just one half). The quasi-rotating zone around the blade is shaped like a cylinder of diameter $D_r = 1$ m, the total total length 0.6 m. The surrounding, stationary zone is also cylindrical, extending 3.5 m in a radial direction, and 2 m and 8 m before and after the rotor.

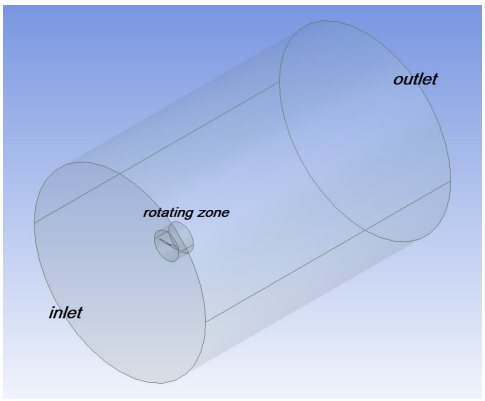

FIGURE 8. Computational domain around the propeller

4.2. Computational grid. After performing a grid independence study, a refined hybrid unstructured mesh that comprises nearly 5.4 million cells was generated and used. Twenty-five layers of prismatic cells encompass the blade walls where the value of dimensionless wall distance y^+ was below 5 in all flow cases. The mesh is additionally refined along the blades and along the interface boundary (that separates the rotating from the stationary zone). Some details of the generated mesh are presented in Fig. 9.

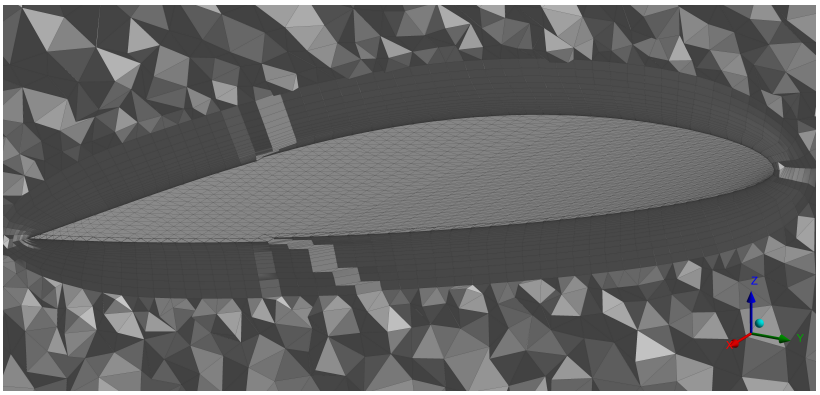

FIGURE 9. Detail of the generated numerical grid

4.3. Numerical set-up. A three-dimensional, incompressible, nearly axisymmetric flow around the blades was modeled by RANS equations and the (quasi-steady) multiple reference frames (MRF) approach. As previously mentioned, flow equations, closed by the $k-\omega$ SST turbulence model, were solved in ANSYS Fluent by the finite volume method [**6**].

Since hovering performances of the rotor are investigated (where velocity infinitely above and below the rotor should be zero), the following boundary conditions are defined. The zero values of gauge pressures along both the inlet and outlet surfaces are assumed, while the blade walls are rotational and no slip. Also, a constant value of angular velocity is assigned to the inner, quasi-rotating zone.

Since air is considered incompressible, a pressure-based solver is used together with the SIMPLEC pressure-velocity coupling scheme. All spatial discretizations were of 2nd order. The computations were performed until the convergence of aerodynamic coefficients was achieved.

4.4. Results and discussion. The CFD approach provides enormous quantities of useful and illustrative data of flow variables. Likewise, Fig. 10 depicts pressure coefficient distribution along the blade in nominal operating conditions. Again, similar to the previous analysis of the blade segment, it can be observed that the flow is mostly smooth, attached and accelerated in the first half of the blade upper surface, while the contribution of the root sections is mostly negligible.

Figure 11 presents the computed velocity contours (in a stationary frame) in the mid-plane. Again, the flow is mostly accelerated (induced) through and after the outer rotor ring. Also, the contraction of the wake behind the rotor is clearly visible. It should be borne in mind that there is no flow coming through the boundaries, and that these velocities are induced solely by the rotor rotation and appropriate geometry.

Figure 12 depicts the tip and root vortices detaching from the blades. They are not significant, and they vanish quickly, implying that the corresponding losses are also acceptable.

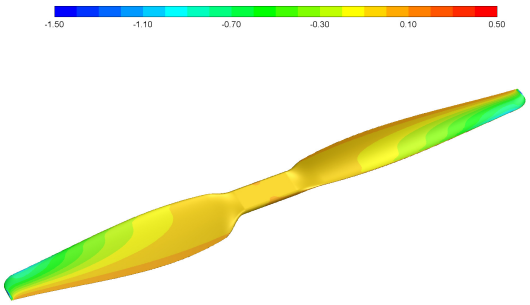

FIGURE 10. Pressure coefficient distribution along the blade at 70% throttle

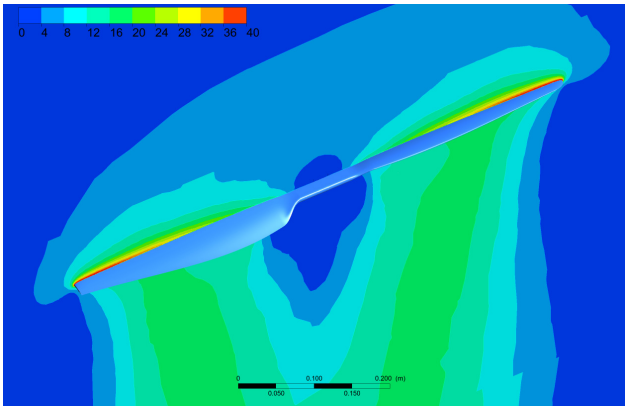

FIGURE 11. Velocity contours in mid-plane at 70% throttle

4.5. Validation of the computational models. Critical estimate of the employed computational model was performed through the comparison with the experimental data gathered by the authors [**1**]. The contrasting of the two sets of data, illustrated in Fig. 13, can be performed by analyzing the corresponding propeller performances, i.e. aerodynamic coefficients of thrust and torque, C_T and C_Q, which are computed as:

$$C_T = \frac{T}{\rho n^2 D^4}, \quad C_Q = \frac{Q}{\rho n^2 D^5},$$

where T and Q denote rotor thrust and torque, respectively, ρ is air density and n is rotor angular frequency.

It should be noted that the torque Q was not actually measured, but implicitly extracted from the values of voltage and current, and with the assumed efficiency of electric-to-mechanical conversion of 82% deduced form the motor datasheets. Still, both curves follow the expected trend and the correspondence between the two sets

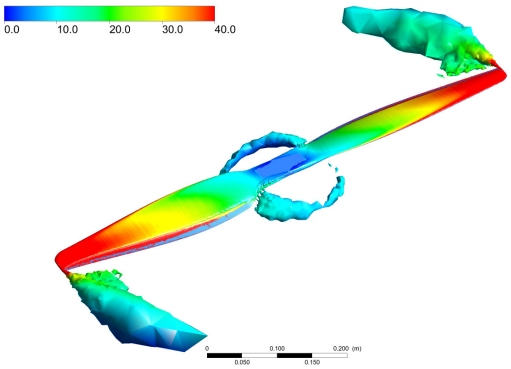

FIGURE 12. Vortical structures separating from blade tips colored by velocity magnitude

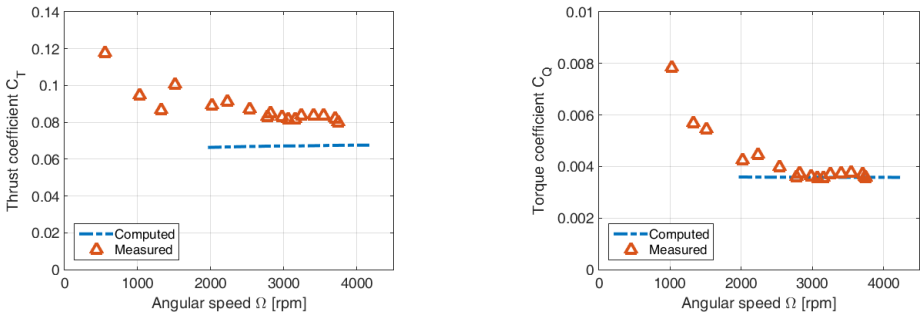

FIGURE 13. Computed aerodynamic coefficients

of results is satisfactory. Interestingly, the estimation of thrust is less accurate (relative differences amount to 15%), implying that the aerodynamic characteristics (and local lift distribution in particular) are slightly underestimated by the employed computational approach and chosen turbulence model. On the other hand, the estimation of torque (and mechanical power) seems to be more reliable implying that drag forces and viscous effects are accounted for to a sufficient degree.

5. Conclusions

This paper provides a brief description of the steps that should be made when simulating flows around small-scale propellers, including both the whole geometry as well as separate segments. Several conclusions can be drawn.

Three-dimensional flows over a propeller blade segment at a Reynolds number of 300,000 and several different angles-of-attack, with the special attention to LSB formation and development, have been studied numerically. Although the LSB phenomenon is still challenging to simulate, various distinctive and illustrative flow visualizations, which present a good starting point for further computational and experimental studies, are provided in the paper.

This paper demonstrates that accurate estimation of airfoil (blade segment) aerodynamic performances at medium and high angles-of-attack and low-Re is extremely difficult. This applies to both numerical and experimental studies, while an analytical approach is barely possible and can only be employed in combination with semi-empirical corrections. On the other hand, correct estimation of aerodynamic characteristics of airfoils is extremely important for further analyses of 3D bodies (wings, blades, etc.) and greatly affects the overall efficiency and the required power. Therefore, a careful and detailed approach should be assumed in flow simulations. For precise results, very fine meshes and unsteady simulations of turbulent flows are necessary. In the end, it is best to validate the obtained numerical data against the results of the corresponding experimental measurements.

On the other hand, if global performances are the main research interest, they can be successfully estimated even by standard computational approaches, as is demonstrated on the flow around the complete propeller geometry. The accuracy and usability of the adopted numerical model are additionally validated against the experimentally obtained data (that includes thrust and torque coefficients). It can be concluded that satisfactory correspondence between the two sets of results can be achieved. Furthermore, numerical estimations seem to be on the safe side, i.e. the required power can be accurately evaluated, while the thrust may be slightly under-estimated (meaning that higher thrust levels can be expected in real flight).

Acknowledgments. The paper is an extended version of the research work presented at the 8$^{\text{th}}$ International Congress of the Serbian Society of Mechanics. It is supported by the Ministry of Education, Science, and Technological Development of the Republic of Serbia through contract no. 451-03-9/2021-14/200105.

References

1. A. Kovačević, J. Svorcan, M. S. Hasan, T. Ivanov, M. Jovanović, *Optimal propeller blade design, computation, manufacturing and experimental testing*, Aircr. Eng. Aerosp. Technol. **93**(8) (2021), 1323–1332.
2. M. K. Herniczek, D. Jee, B. Sanders, R. Feszty, *Rotor blade optimization and flight testing of a small UAV rotorcraft*, J. Unmanned Veh. Syst. **7**(4) (2019), 325–344.
3. M. A. J. Kuitche, R. M. Botez, R. Viso, J. C. Maunand, O. C. Moyao, *Blade element momentum new methodology and wind tunnel test performance evaluation for the UAS-S45 Balaam propeller*, CEAS Aeronaut. J. **11**(4) (2020), 937–953.
4. E. Vargas Loureiro, N. L. Oliveira, P. H. Hallak, F. de Souza Bastos, L. M. Rocha, R. Grande Pancini Delmonte, A. C. de Castro Lemonge, *Evaluation of low fidelity and CFD methods for the aerodynamic performance of a small propeller*, Aerosp. Sci. Technol. **108** (2021), 106402.
5. M. Figat, P. Piatkowska, *Numerical investigation of mutual interaction between a pusher propeller and a fuselage*, Proc. Inst. Mech. Eng. G J. Aerosp. Eng. **235**(1) (2021), 40–53.
6. *ANSYS Fluent Theory Guide*, ANSYS, Inc., Canonsburg, 2017.
7. R. Langtry, F. Menter, *Transition modeling for general CFD applications in aeronautics*, in: 43$^{\text{rd}}$ AIAA Aerospace Sciences Meeting and Exhibit, 2005, AIAA 2005-522.
8. F. R. Menter, Y. Egorov, *The scale-adaptive simulation method for unsteady turbulent flow predictions. Part 1: Theory and model description*, Flow Turbul. Combust. **85**(1) (2010), 113–138.
9. F. R. Menter, *Best Practice: Scale-Resolving Simulations in ANSYS CFD*, ANSYS, Inc., Canonsburg, 2012.

10. C. D. Argyropoulos, N. C. Markatos, *Recent advances on the numerical modelling of turbulent flows*, Appl. Math. Modelling **39** (2015), 693–732.
11. B. Chaouat, *The state of the art of hybrid RANS/LES modeling for the simulation of turbulent flows*, Flow Turbul. Combust. **99** (2017), 279–327.
12. M. Drela, *XFOIL: an analysis and design system for low Reynolds number airfoils*, in: T. J. Mueller (ed.), *Low Reynolds Number Aerodynamics*, Springer, Berlin, Heidelberg, 1989, 1–12.
13. Y. Zhiyin *Large-eddy simulation: Past, present and the future*, Chin. J. Aeronaut. **28**(1) (2015), 11–24.
14. J. W. Kurelek, B. A.Tuna, S. Yarusevych S, M. Kotsonis, *Three-dimensional development of coherent structures in a two-dimensional laminar separation bubble*, AIAA J. **59(2)** (2021), 493–505.
15. H. Aminaei, A. R. Mostofizadeh, M. Dehghan Manshadi, *Experimental and numerical study of wing boundary layer behavior in propeller flowfield*, J. Vis. **22**(3) (2019), 489–503.
16. V. Golubev, *Recent advances in acoustics of transitional airfoils with feedback-loop interactions: A review*, Appl. Sci. **11**(2) (2021), 1057.
17. O. Erkan, M. Ozkan, T. H. Karakoc, S. J. Garrett, P. J. Thomas, *Investigation of aerodynamic performance characteristics of a wind-turbine-blade profile using the finite-volume method*, Renew. Energ. **161** (2020), 1359–1367.
18. V. Somashekar, A. Immanuel Selwyn Raj, *Numerical and experimental study of the laminar separation bubble over SS007 airfoil for micro aerial vehicles*, Aircr. Eng. Aerosp. Technol. **92**(8) (2020), 1125–1131.

О ИЗВОДИВИМ СИМУЛАЦИЈАМА ОПСТРУЈАВАЊА МАЛИХ РОТОРА И СЕГМЕНАТА ЛОПАТИЦА

Резиме. Рад је усмерен ка могућностима спровођења задовољавајућих симулација комплексних струјних поља која се јављају око малих елиса вишероторних летелица. Популарност таквих беспилотних летелица је у сталном порасту због њихових разнородних намена (надзор, комуникација, испоруке, итд) те се и потреба за успешним (употребљивим, задовољавајућим, практичним) нумеричким алатом такође нагло повећава. Са инжењерског становишта, важно је добити процене величина струјног поља задовољавајуће тачности у реалном времену да би процес пројектовања могао бити брз и ефикасан, нарочито због анализа које следе (структуралних и динамике лета). Из тог разлога, најчешће се користе и валидирају релативно стандардни модели нпр. Навије-Стоксове једначине осредњене Рејнолдсовом статистиком, а решене методом коначних запремина. Са друге стране, требало би обратити нарочиту пажњу на различите посебности струјног поља које се дешавају око сегмената лопатице обликованих као аеропрофили јер се оваква струјања одликују малим тетивама (дужинама), малим брзинама, па и малим Рејнолдсовим бројевима и израженим вискозним ефектима. Истраживана струјања при малим Рејнолдсовим бројевима подразумевају и прелазне и зоне турбулентног струјања, ламинарне мехурове, отцепљење струјања, као и ротирајуће вртложне трагове, што захтева донекле специфични приступ моделирању струјања (напредније турбулентне моделе, фине просторне и временске размере, итд). Овде су приказани и појашњени спроведени прорачуни (око непокретног сегмента лопатице као и обртне елисе), који су затворени различитим турбулентним моделима. Разни квалитативни и квантитативни разултати су дати, упоређени и продискутовани. Споменуте су основне могућности и ограничења сваког прорачунског приступа. Где је било могуће, нумерички подаци валидирани су кроз поређење са експерименталним. Слагања између два скупа резултата се могу сматрати задовољавајућим (релативне разлике у коефицијентима вучне силе не прелазе 15%, док су још и мање за коефицијенте момента). Може се закључити да одабир турбулентног модела веома утиче на крајње резултате, чак и у номиналним радним режимима (при средњим вредностима нападног угла где доминира ламинарно, прилепљено струјање). Карактеристични струјни феномени су и ту присутни, и да би били адекватно симулирани, потребно је усвојити свеобухватан нумерички приступ.

Department of Aeronautics
University of Belgrade, Faculty of Mechanical Engineering
Belgrade
Serbia
jsvorcan@mas.bg.ac.rs

akovacevic@mas.bg.ac.rs

dtanovic@mas.bg.ac.rs

sakibhasan89@yahoo.com

(Received 11.10.2021.)
(Revised 27.10.2021.)
(Available online 18.11.2021.)